AGU PUBLICATIONS

Paleoceanography

RESEARCH ARTICLE
10.1002/2013PA002599

Key Points:
- Multiproxy records of West Pacific precipitation changes over the past 120 ka
- Precipitation variability is influenced by precessional insolation forcing
- Oxygen isotope variability is driven by regional hydrology

Supporting Information:
- Readme
- Table S1
- Text S1
- Figure S1
- Figure S2
- Figure S3
- Figure S4

Correspondence to:
N. Fraser,
nf@gpi.uni-kiel.de

Citation:
Fraser, N., W. Kuhnt, A. Holbourn, T. Bolliet, N. Andersen, T. Blanz, and L. Beaufort (2014), Precipitation variability within the West Pacific Warm Pool over the past 120 ka: Evidence from the Davao Gulf, southern Philippines, *Paleoceanography*, *29*, 1094–1110, doi:10.1002/2013PA002599.

Received 19 DEC 2013
Accepted 20 OCT 2014
Accepted article online 24 OCT 2014
Published online 21 NOV 2014

Precipitation variability within the West Pacific Warm Pool over the past 120 ka: Evidence from the Davao Gulf, southern Philippines

Nicholas Fraser[1], Wolfgang Kuhnt[1], Ann Holbourn[1], Timothé Bolliet[2], Nils Andersen[3], Thomas Blanz[1], and Luc Beaufort[4]

[1]Institute of Geosciences, Christian-Albrechts Universität zu Kiel, Kiel, Germany, [2]Laboratoire des Sciences du Climat et de l'Environnement (IPSL), CNRS-CEA-UVSQ, Gif-sur-Yvette, France, [3]Leibniz-Laboratory for Radiometric Dating and Isotope Research, Christian-Albrechts Universität zu Kiel, Kiel, Germany, [4]CEREGE, CNRS-Université Aix-Marseille, Aix-en-Provence, France

Abstract Proxy records of hydrologic variability in the West Pacific Warm Pool (WPWP) have revealed wide-scale changes in past convective activity in response to orbital and suborbital climate forcings. However, attributing proxy responses to regional changes in WPWP hydrology versus local variations in precipitation requires independent records linking the terrestrial and marine realms. We present high-resolution stable isotope, $U^{K'}_{37}$ sea surface temperature, X-ray fluorescence (XRF) core scanning, and coccolithophore-derived paleoproductivity records covering the past 120 ka from International Marine Global Change (IMAGES) Program Core MD06-3075 (6°29′N, 125°50′E, water depth 1878 m), situated in the Davao Gulf on the southern side of Mindanao. XRF-derived log(Fe/Ca) records provide a robust proxy for runoff-driven sedimentary discharge from Mindanao, while past changes in local productivity are associated with variable freshwater runoff and stratification of the surface layer. Significant precessional-scale variability in sedimentary discharge occurred during marine isotope stage (MIS) 5, with peaks in discharge contemporaneous with Northern Hemisphere summer insolation minima. We attribute these changes to the latitudinal migration of the Intertropical Convergence Zone (ITCZ) over the WPWP together with variability in the strength of the Walker circulation acting on precessional timescales. Between 60 and 15 ka sedimentary discharge at Mindanao was muted, displaying little orbital- or millennial-scale variability, likely in response to weakened precessional insolation forcing and lower sea level driving increased subsidence of air masses over the exposed Sunda Shelf. These results highlight the high degree of local variability in the precipitation response to past climate changes in the WPWP.

1. Introduction

The West Pacific Warm Pool (WPWP) forms one of the world's largest and most important centers of tropical convection, supplying heat and moisture to the midlatitudes and high latitudes, and playing an active role in global climate dynamics [*Cane*, 1998; *Hoerling et al*., 2001]. Pressure gradients between the eastern subtropical Pacific and the Australian and Indonesian maritime landmasses drive easterly trade winds which push warm surface waters westward and result in a large zonal sea surface temperature (SST) gradient between the eastern and western tropical Pacific. This feedback mechanism reinforces convergence of wind and surface waters in the West Pacific, resulting in permanent year-round warm pool where SSTs exceed 28°C. By way of comparison, SSTs in the Eastern Equatorial Pacific average 25 to 27°C due to upwelling induced by equatorial trade winds [*Bjerknes*, 1969].

The Intertropical Convergence Zone (ITCZ), a narrow band of convective winds and intense precipitation situated close to the equator, migrates seasonally over the WPWP in response to interhemispheric temperature gradients [*Schneider et al*., 2014]. During boreal summer, the ITCZ migrates northward, resulting in high precipitation over China and the northern regions of the Indonesian archipelago, while southern Indonesia and Australia experience relatively dry conditions. The opposite effect occurs during boreal winter. These patterns of precipitation are closely linked with the East-Asian Monsoon (EAM) and Indo-Australian Monsoon systems. Variability in the El Niño–Southern Oscillation (ENSO) acting on irregular 2 to 10 year timescales also has a direct influence on WPWP convection; during strong El Niño years a breakdown in the

Walker circulation causes weakened easterly trade winds and a shift in the center of tropical convection toward the Central Pacific, resulting in a net reduction in precipitation over the Indonesian landmass [*Ropelewski and Halpert*, 1987]. During La Niña years, the opposite effect is observed, with a warmer WPWP extending further toward East Asia, driving enhanced rainfall over this region.

During the late Pleistocene, paleoclimate records of past convective activity in the tropics show a strong sensitivity to precessional cyclicity. Records from the Northern (Southern) Hemisphere typically indicate a reduction in precipitation during Northern (Southern) Hemisphere summer insolation maxima, when perihelion occurs close to summer solstice [e.g., *Wang et al*., 2001, 2007, 2008; *Cruz et al*., 2005; *Tachikawa et al*., 2011; *Meckler et al*., 2012; *Cheng et al*., 2012]. Such patterns implicate changes in the seasonal distribution of insolation between the Northern and Southern Hemispheres as a control on past precipitation variability, which can be attributed to meridional "shifts" of the local summer ITCZ position associated with changes in cross-equatorial heat transport [*Donohoe et al*., 2013; *McGee et al*., 2014] and to thermodynamic changes in humidity and moisture advection between hemispheres [*Merlis et al*., 2013]. Abrupt Northern Hemisphere climate signals such as Dansgaard-Oeschger interstadials and Heinrich stadials, which are documented in Greenland ice cores (e.g., GISP2), are furthermore imprinted upon these orbital-scale trends from the WPWP [e.g., *Wang et al*., 2001; *Stott et al*., 2002; *Dannenmann et al*., 2003; *Saikku et al*., 2009; *Carolin et al*., 2013; *Ayliffe et al*., 2013; *Denniston et al*., 2013] and are consistent with a northward (southward) meridional displacement of the ITCZ in response to Northern Hemisphere warming (cooling). Persistent changes in zonal circulation patterns associated with the Walker circulation and mean ENSO conditions have also been posited as important controls on proxy records of convection from both the East and West Pacific [*Tudhope et al*., 2001; *Beaufort et al*., 2001; *Stott et al*., 2002; *Koutavas et al*., 2002; *Martinez et al*., 2003; *Turney et al*., 2004], a finding that has been replicated in recent modeling approaches [*DiNezio et al*., 2011; *DiNezio and Tierney*, 2013].

Thus far, most reconstructions of past convective variability in the WPWP have focused upon oxygen isotope ($\delta^{18}O$) records from speleothems [*Partin et al*., 2007; *Griffiths et al*., 2009; *Meckler et al*., 2012; *Carolin et al*., 2013; *Ayliffe et al*., 2013; *Denniston et al*., 2013] and $\delta^{18}O$ records of surface seawater ($\delta^{18}O_{sw}$) derived from planktonic foraminifera [*Stott et al*., 2002; *Medina-Elizalde and Lea*, 2005; *de Garidel-Thoron et al*., 2007; *Saikku et al*., 2009; *Gibbons et al*., 2014]. These isotopic records primarily reflect large-scale hydrologic variability rather than local precipitation changes [*Gibbons et al*., 2014] and require an understanding of the roles of evaporation feedbacks and source water $\delta^{18}O$ on the $\delta^{18}O$ signal recorded in surface seawater and cave drip water. Resolving local precipitation patterns in the WPWP therefore require detailed, independent proxy records which are not influenced by widespread regional changes. Here we present a multiproxy record combining foraminiferal $\delta^{18}O$, X-ray fluorescence (XRF)-derived sedimentary runoff, and coccolithophore-based $U^{K'}_{37}$ sea surface temperature (SST) and paleoproductivity estimates from Core MD06-3075 located in the Davao Gulf (06°28.6 N, 125°49.9 E, 1878 m water depth), 50 km off the coast of Mindanao (Figure 1). This sheltered bay sits within the WPWP on the eastern side of the Indonesian archipelago and provides a favorable location for linking marine and terrestrial records of precipitation and runoff, and monitoring past climatic changes related to the evolution of the WPWP over the late Pleistocene.

2. Materials and Study Area

Core MD06-3075 was retrieved with a Calypso piston corer during the Marco Polo II cruise aboard the *Marion Dufresne* in June 2006, as part of the IMAGES coring program [*Laj and Shipboard Scientific Party*, 2006]. It is composed of 30.75 m of homogenous dark olive grey silty clay, interrupted by irregular dispersed ash layers (1 to 5 cm thick). Additionally, a gap in the core is noted between 192 and 208 cm, due to the presence of a large piece of broken core liner. The coring location was chosen due to its position on a topographic high, reducing the likelihood of turbidite deposition (Figure 1). The Davao Gulf acts as a catchment basin for several large rivers from Mindanao, most notably the Davao River, making this site ideally placed to capture precipitation-induced runoff signals from Mindanao. The majority of thermocline waters at this site originate from the North Equatorial Current [*Toole et al*., 1990], while the intermediate circulation is dominated by Antarctic Intermediate Water, which passes over a shallow sill (~800 m depth) extending southward from Mindanao [*Qu et al*., 1999; *Kashino et al*., 1996] (Figure 1).

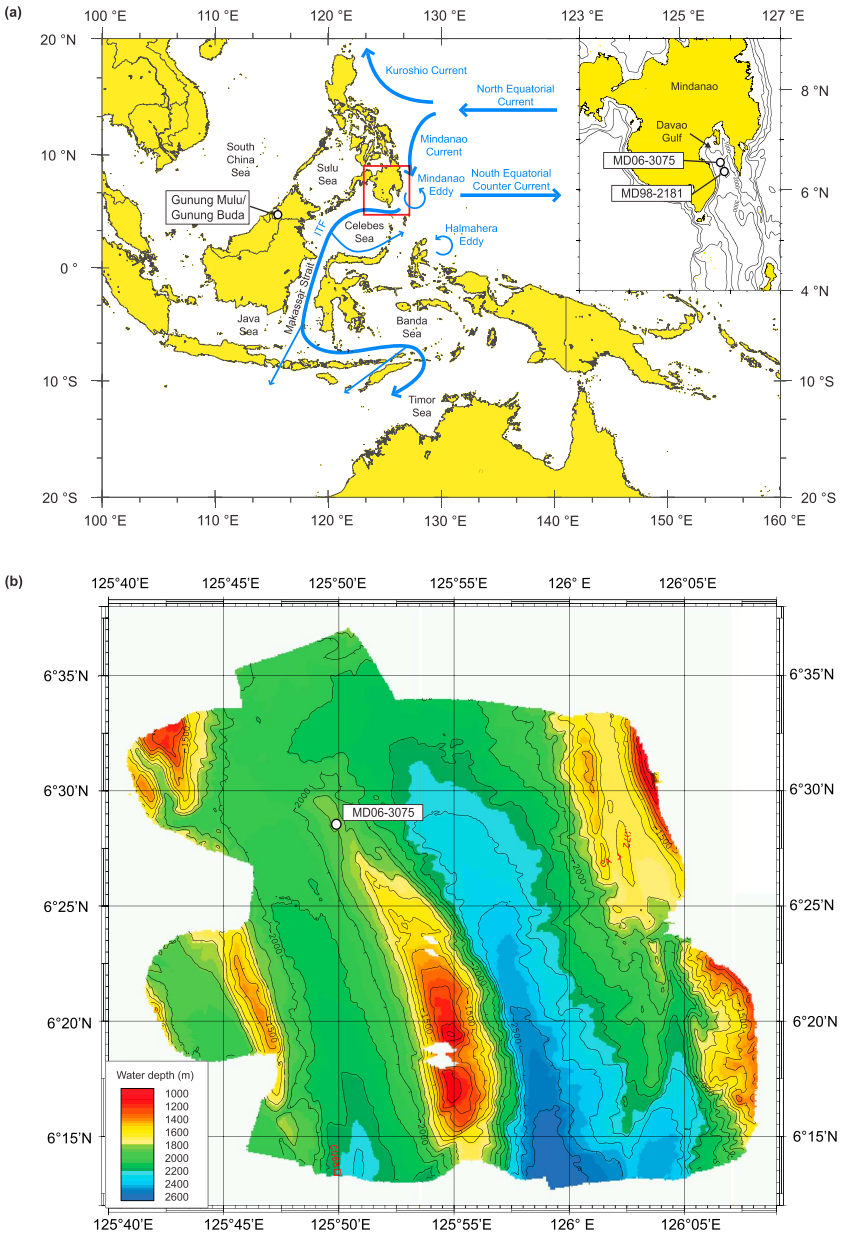

Figure 1. (a) Location map of Cores MD06-3075 (this study) and MD98-2181 [*Stott et al*., 2002, 2007; *Saikku et al*., 2009], and speleothem records from Gunung Buda/Gunung Mulu Caves, Borneo [*Partin et al*., 2007; *Meckler et al*., 2012; *Carolin et al*., 2013]. The main oceanic currents acting in the WPWP region are shown by blue arrows. (b) Bathymetric map of the Davao Gulf including the coring position of Core MD06-3075 [*Laj and Shipboard Scientific Party*, 2006].

The core site sits within the center of the modern-day WPWP, with an annual average SST of 28.7°C. SSTs are highest in boreal summer, above 29°C, and cool by approximately 1 to 1.5°C in boreal winter (Figure 2b). Seasonal precipitation and wind patterns are linked with the migration of the ITCZ. Precipitation is highest (>4.5 mm/d) when a northern-positioned ITCZ induces convergence over Mindanao between June and October, and lowest (<4 mm/d) when the ITCZ is positioned to the south between February and April (Figure 2b). However, this seasonal cycle of precipitation is relatively weak compared to the extreme monsoonal precipitation cycles found in northern Australia or southern China, since the core site is positioned relatively centrally within the latitudinal range of the maximum northward and southward ITCZ position. Oxygen isotopes of precipitation falling in Mindanao show generally lower values between June and September, and higher values between January and May, likely caused by changing wind directions and

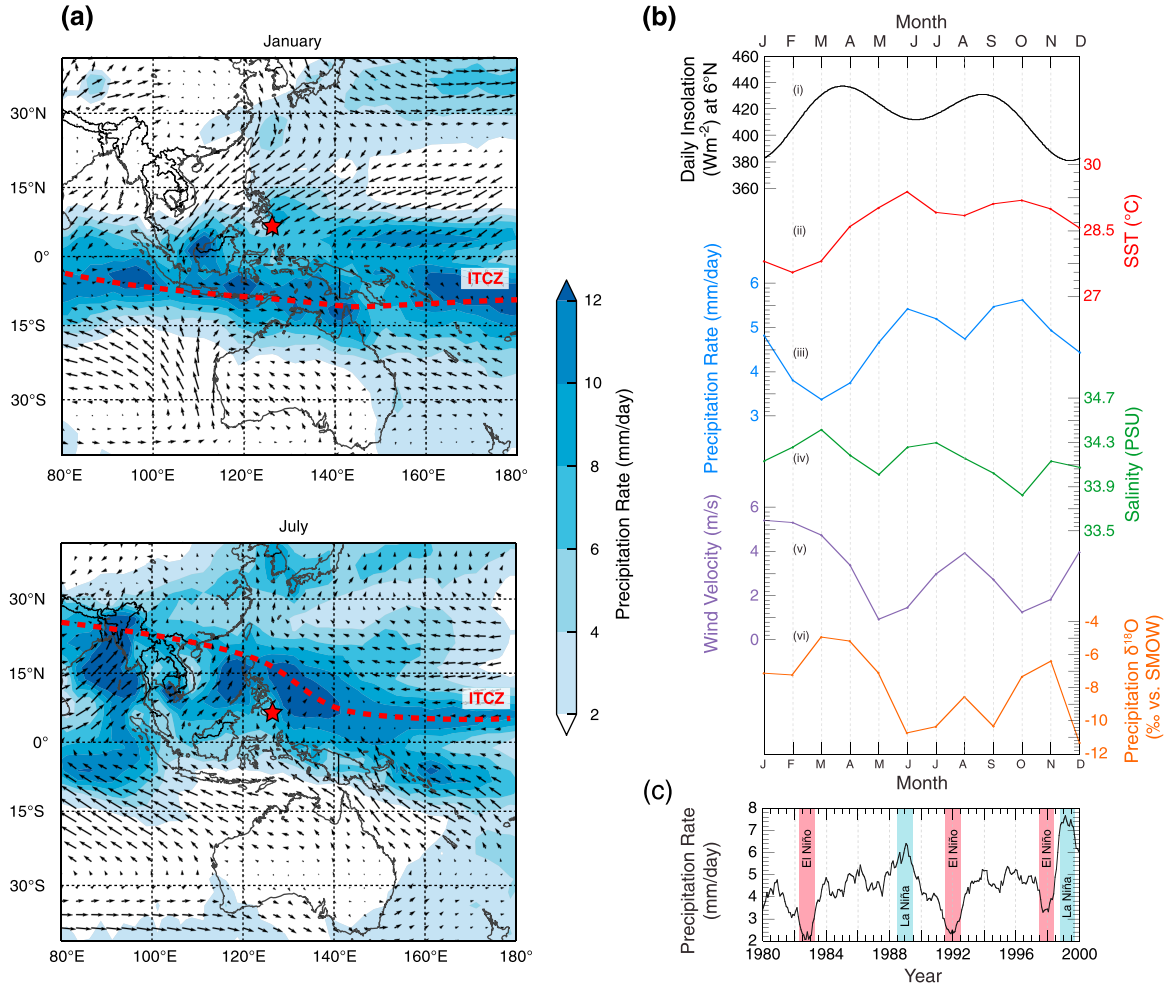

Figure 2. (a) Wind and precipitation rates in the WPWP during January (top) and July (bottom). Wind data are derived from the National Centers for Environmental Prediction (NCEP) reanalysis project, available at http://www.esrl.noaa.gov/psd/. Precipitation data were extracted from the *Xie and Arkin* [1997] Climate Prediction Center Merged Analysis of Precipitation (CMAP) precipitation estimates available at http://iridl.ldeo.columbia.edu. Red dashed line represents the mean monthly position of the ITCZ, following *Waliser and Gautier* [1993]. Location of Core MD06-3075 is shown by a red star. (b) Monthly climatology in the Davao Gulf showing: (i) insolation at 6°N, (ii) average SST (World Ocean Atlas 2009) [*Locarnini et al.*, 2010], (iii) average precipitation rates (extracted from the *Xie and Arkin* [1997] CMAP precipitation estimate available at http://iridl.ldeo.columbia.edu/), (iv) average salinity (World Ocean Atlas 2009) [*Antonov et al.*, 2010], (v) average wind velocities (NCEP reanalysis data at http://www.esrl.noaa.gov/psd/), and (vi) $\delta^{18}O$ measured in precipitation (Global Network of Isotopes in Precipitation) [*International Atomic Energy Agency/World Meteorological Organization*, 2013] across a composite of five stations situated in southern Mindanao. (c) Average precipitation rates over the 1980–2000 period with strongest El Niño (red bars) and La Niña (blue bars) years based on NINO3.4 index anomalies.

associated changes in the sources and transport pathways of atmospheric vapor (Figure 2b). Precipitation records from the past decades in the Davao Gulf also indicate the important effect ENSO has at this location; during strong El Niño years, precipitation is suppressed and Mindanao experiences generally dry conditions, while during La Niña years, the reverse situation occurs (Figure 2c).

3. Methods

3.1. Accelerator Mass Spectrometry ^{14}C Dating

For accelerator mass spectrometry (AMS) ^{14}C dating, approximately 600 to 800 well-preserved tests of the near-surface dwelling planktonic foraminifera *Globigerinoides ruber* were picked from the >250 μm size fraction, where abundance allowed. In instances of low abundance, mixed planktonic samples consisting of *Globigerinoides ruber*, *Globigerinoides sacculifer*, and *Pulleniatina obliquiloculata* were analyzed. AMS ^{14}C dating was performed at the Leibniz Laboratory, Kiel University, following the protocol described by *Nadeau et al.* [1997]

and *Schleicher et al*. [1998]. Conventional ages were converted to calendar ages following *Fairbanks et al*. [2005], after applying a reservoir age correction of 480 years for samples younger than 13 ka, and 630 years for older samples, consistent with other recent studies in this region [e.g., *Saikku et al*., 2009; *Bolliet et al*., 2011].

3.2. Stable Isotope Analysis

For $\delta^{18}O$ analysis, approximately 10 tests of *G. ruber*, and between 1 and 5 tests of the benthic species *Planulina wuellerstorfi* were picked at 10 cm intervals. Over the upper 900 cm of the core, the spacing of the *G. ruber* sampling intervals was decreased to 2 cm. In rare cases where *P. wuellerstorfi* was absent, *Cibicidoides pachyderma* or *Uvigerina* spp. were used. *Cibicidoides* and *Planulina* calcify with $\delta^{18}O$ values at or close to isotopic equilibrium with ambient seawater [*Bemis et al*., 1998; *Marchitto et al*., 2014], while *Uvigerina* spp. require an additional correction of −0.47‰ (following *Marchitto et al*. [2014]), to bring values in line with isotopic equilibrium values of ambient seawater. Samples were crushed into fragments under the microscope to ensure all chambers were open, then agitated in ethanol in an ultrasonic bath for several seconds, and dried at 40°C. Stable oxygen isotopes were measured with the Finnigan MAT 253 mass spectrometer at the Leibniz Laboratory, Kiel University. The system is coupled to a Carbo-Kiel Device (Type IV) for automated CO_2 preparation from carbonate samples for isotopic analysis. Samples were reacted by individual acid addition (99% H_3PO_4 at 75°C). Standard external error is better than ±0.09‰. Replicate measurements on 25 pairs of *G. ruber* indicate a reproducibility (1σ) of ±0.11‰ for $\delta^{18}O$, while replicate measurements on 17 paired benthic foraminifera samples indicate a reproducibility (1σ) of ±0.10‰.

3.3. XRF Core Scanning

The archive half of the core was scanned for major element intensities in 1 cm resolution at the Marum Center, University of Bremen using the Avaatech core scanner. Intensities of elements common in continental siliciclastic rocks, especially clays (e.g., Ti, Fe, and Al), are used as qualititative proxies for land-derived sedimentary discharge [*Arz et al*., 1998], and thus XRF records serve as a proxy for precipitation-induced runoff. Measured intensities are normalized by calcium and presented as log ratios to reduce matrix effects [*Aitchison*, 1982; *Weltje and Tjallingii*, 2008].

3.4. Coccolith Counts

Coccoliths were counted at 10 cm resolution following the procedure outlined in *Bolliet et al*. [2011]. Six taxa dominate the assemblage: *Emiliania huxleyi*, *Florisphaera profunda*, *Gephyrocapsa oceanica*, *Gephyrocapsa ericsonii*, *Gephyrocapsa muellerae*, and *Helicosphaera* spp. Coccolithophore assemblages have been shown to be reliable indicators of oceanic productivity [*Beaufort et al*., 1997]. In particular, the relative abundance of the lower photic zone (150 to 200 m water depth) dwelling species *F. profunda* has been related to the depth of the nutricline [*Molfino and McIntyre*, 1990; *Beaufort et al*., 1997; *Andruleit and Rogalla*, 2002]; when the nutricline is shallow, the upper photic zone dwelling species dominate coccolith assemblages [*Molfino and McIntyre*, 1990] while the opposite situation occurs when the nutricline deepens. The relative abundance of *F. profunda* (%*Fp*) has been successfully calibrated to primary productivity (PP, gC m^{-2} yr^{-1}) by *Beaufort et al*. [1997] in the Indian Ocean, resulting in the equation applied in this study:

$$PP = 617 - [279 \times \log(\%Fp + 3)]$$

3.5. Carbonate Content

Carbonate content was measured on dried and crushed bulk sediment by full reaction with 6 N HCl using a "carbonate bomb" device [*Müller and Gastner*, 1971] at the University of Kiel. Samples were measured at 30 cm resolution throughout the core. Standard error of the carbonate bomb device is ±1%.

3.6. $U^{K'}_{37}$ SST Estimates

SSTs were estimated at 10 cm resolution using the alkenone-based $U^{K'}_{37}$ proxy. Alkenones were extracted from 1 g of homogenized bulk sediments and analyzed with double-column gas chromatography at the University of Kiel, following the procedure fully outlined in *Rincón-Martínez et al*. [2010]. We calibrated measured $U^{K'}_{37}$ to temperature following *Sonzogni et al*. [1997] (see supporting information for further discussion), which has been developed for high temperature (24–29°C) core tops from the Indian Ocean with the equation:

$$U^{K'}_{37} = (0.023 \text{ x } SST(°C)) + 0.316$$

3.7. Calculation of Seawater $\delta^{18}O$ ($\delta^{18}O_{sw}$)

Surface $\delta^{18}O_{sw}$ was calculated from $\delta^{18}O$ measurements on *G. ruber* and $U^{K'}_{37}$ temperatures from the same sample depth. Differences in seasonal growth patterns and ecologies of $\delta^{18}O$-recording foraminifera and $U^{K'}_{37}$-recording coccolithophores [cf. *Timmermann et al*., 2014] could introduce uncertainty into calculated $\delta^{18}O_{sw}$, where SSTs would preferentially be measured on Mg/Ca from paired foraminifera samples. However, a temperature bias of ~5°C would be required to produce a shift in $\delta^{18}O_{sw}$ of ~1‰, which is significantly larger than maximum temperature bias that have been observed between Mg/Ca and $U^{K'}_{37}$ SST reconstructions in this region, and thus the effect on the long-term variability of $\delta^{18}O_{sw}$ is assumed to be small. The equation of *Bemis et al*. [1998] was used for the calculation:

$$\delta^{18}O_{sw\ (versus\ SMOW)} = 0.27 + \left(SST\ (°C) - 16.5 + \left(4.8 \times \delta^{18}O_{(versus\ PDB)}\right)\right)/4.8$$

After calculation of $\delta^{18}O_{sw}$, a correction was applied to the samples to remove the $\delta^{18}O$ signal associated with the global ice volume effect [*Waelbroeck et al*., 2002].

4. Results

4.1. Chronology

The age model for Core MD06-3075 (Table S1 in the supporting information) is based upon 16 reservoir-corrected AMS ^{14}C age dates in the upper core to a depth of 970 cm, approximately 31 ka (Figure 3). Below 970 cm, the age model was generated by correlation of benthic oxygen isotope data to the EDML1 (European Project for Ice Coring in Antarctica (EPICA) ice core from Dronning Maud Land) chronology developed for the EPICA ice core from Dronning Maud Land (EDML) by *Ruth et al*. [2007]. Nine tie points were used between Core MD06-3075 and EDML1 to constrain ages between 31 and 116 ka. The final age model was generated by linear interpolation between AMS ^{14}C ages and tie points. High-sedimentation rates in the upper ~5 m of the core are likely artificially introduced by sediment oversampling caused by the piston coring system [*Széréméta et al*., 2004]. Below 5 m, sedimentation rates vary between 8 and 38 cm/kyr.

4.2. Stable Isotopes

Benthic $\delta^{18}O$ records show well-defined glacial-interglacial isotopic stages with fluctuations in $\delta^{18}O$ between 2.5 and 4.2‰, and a maximum amplitude of 1.7‰ over Termination I (Figure 4). A transition from values of ~2.8‰ to ~3.8‰ in the oldest part of the core likely represents the transition between marine isotope stage (MIS) 5e and 5d. The four other main substages of MIS 5 are additionally identified (a–d). The $\delta^{18}O$ records from *G. ruber* also show the main glacial-interglacial cycles as seen in the benthic record (Figure 4), with values fluctuating between −3.2 and −0.8‰, and a maximum amplitude of ~2.2‰ over Termination I. During MIS 5, *G. ruber* $\delta^{18}O$ varies between −2.7 and −1.6‰, prior to a significant increase during the cold MIS 4 period where values reach a maximum of −1.1‰. During MIS 3, values fluctuate between −1.9 and −1.0‰, though the resolution in this portion of the record is too low to attribute these variations to individual Dansgaard-Oeschger interstadials and Heinrich stadials. $\delta^{18}O$ values decrease rapidly between ~18 and 13 ka (from −0.8 to −2.0‰), before a brief excursion to more positive values representing the Younger Dryas (YD, ~12.8–11.5 ka) cooling event (Figure 2 in the supporting information). $\delta^{18}O$ continues to decrease at a reduced rate throughout the Holocene, reaching a minimum in the late Holocene with values of ~ −3.0‰, including a core top value of −3.1‰.

4.3. SST Record

$U^{K'}_{37}$-derived temperatures suggest an SST range of 25.3°C to 29.2°C with a deglacial warming amplitude of 3.4°C (Figure 4). An average of the upper three Holocene measurements gives a core top SST estimate of 28.7°C, consistent with modern-day annual SSTs at our locality (28.7°C) [*Locarnini et al*., 2010]. Temperature maxima during MIS 5a, 5c, and latest 5e are found to be in excess of those in the Holocene by ~0.5°C, and the variability between MIS 5 substages is on the order of 1.5°C. The coolest temperatures are found at ~18 ka, at the beginning of Heinrich Stadial 1 (HS1, ~18–14.6 ka). A temperature plateau at 27.2°C is consistent with the timing of the Bølling-Allerød (BA, ~14.6–12.8 ka) period, while the YD is punctuated by a brief cooling episode (Figure S2 in the supporting information). An additional cooling episode is observed in the late Holocene between 2 and 1 ka, with temperatures ~0.9°C cooler than those between 5 and 2 ka and between 1 and 0 ka.

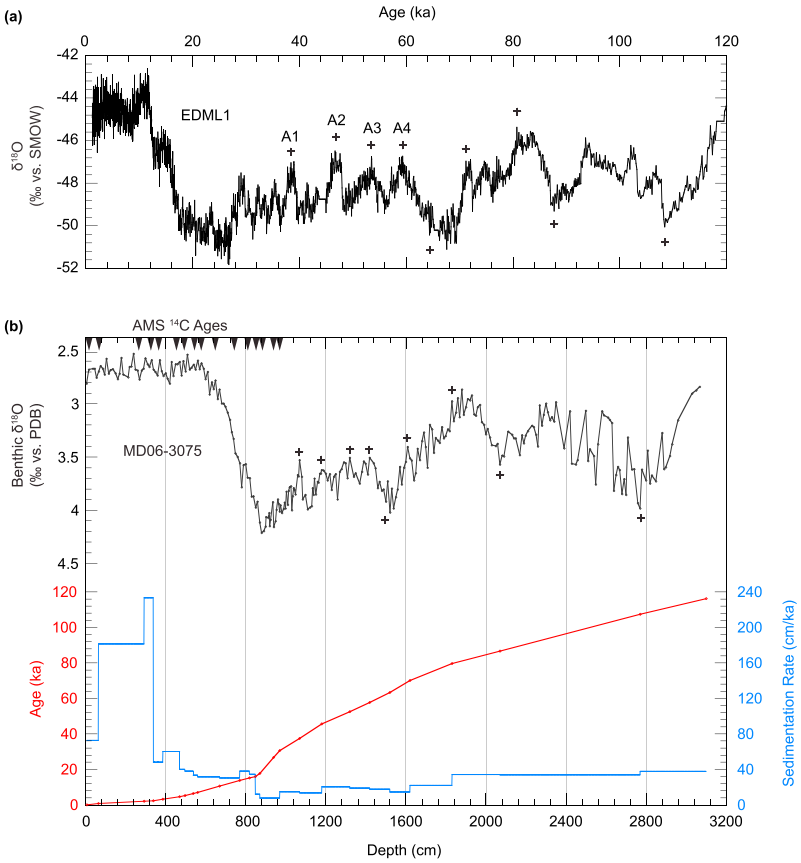

Figure 3. Age model development for Core MD06-3075 (data available in Table S1 in the supporting information). (a) EDML1 chronology for the past 120 kyr based upon the $\delta^{18}O$ record for the EPICA ice core from Dronning Maud Land (EDML1) by *Ruth et al*. [2007]. (b) Benthic $\delta^{18}O$ (black line) and sedimentation rates (green line) versus depth for Core MD06-3075. Red line displays the final age model. Arrows indicate sample depths for AMS ^{14}C analysis. Crosses indicate tie points with the EDML1 chronology.

4.4. $\delta^{18}O_{sw}$ Reconstructions

$\delta^{18}O_{sw}$ was calculated from $\delta^{18}O_{calcite}$ of the near-surface dwelling foraminifera *G. ruber*, corrected for temperature and ice volume effects. Resulting near-surface $\delta^{18}O_{sw}$ shows maximum variability between ~−0.3‰ and ~1‰ (Figure 5), with a core top $\delta^{18}O_{sw}$ value of −0.28‰. $\delta^{18}O_{sw}$ shows a component of precessional-scale variability during MIS 5 and 4, with lower values during Northern Hemisphere insolation minima, although these trends are imprinted by significant millennial-scale variability. A distinct maximum with values close to 1‰ is reached during late MIS 4, preceding a long-term decreasing trend that continues until the present day, where values reach their minimum at ~−0.3‰. A prominent negative excursion in $\delta^{18}O_{sw}$ during the BA period interrupts the long-term increasing trend from the Last Glacial Maximum (LGM) to present.

4.5. XRF Core Scanning

In this study we use log(Fe/Ca) as a proxy for terrigenous-derived versus marine-derived sediment composition. Raw counts of elements Ca, Fe, Ti, Al, Si, and K indicate that Fe represents a major element (Figure S3 in the supporting information). Counts of Al, Si, and K show differing long-term trends to Fe and Ti, which may indicate a different source or continental weathering mechanism for these elements. *Tjallingii et al*. [2007] have demonstrated that pore water contents can have a large impact on XRF intensities of some lighter elements, such as Al and Si, which may make their usage as indicators for runoff unsuitable. Orbital-scale fluctuations in log(Fe/Ca) are noted during MIS 4 and 5, with lower values exhibited between 105–98 ka, 82–76 ka, and 64–60 ka (Figure 5). During the globally cool period between 60 ka and 20 ka, log(Fe/Ca) remains relatively low and stable and does not display significant millennial-scale variability. A slight increase

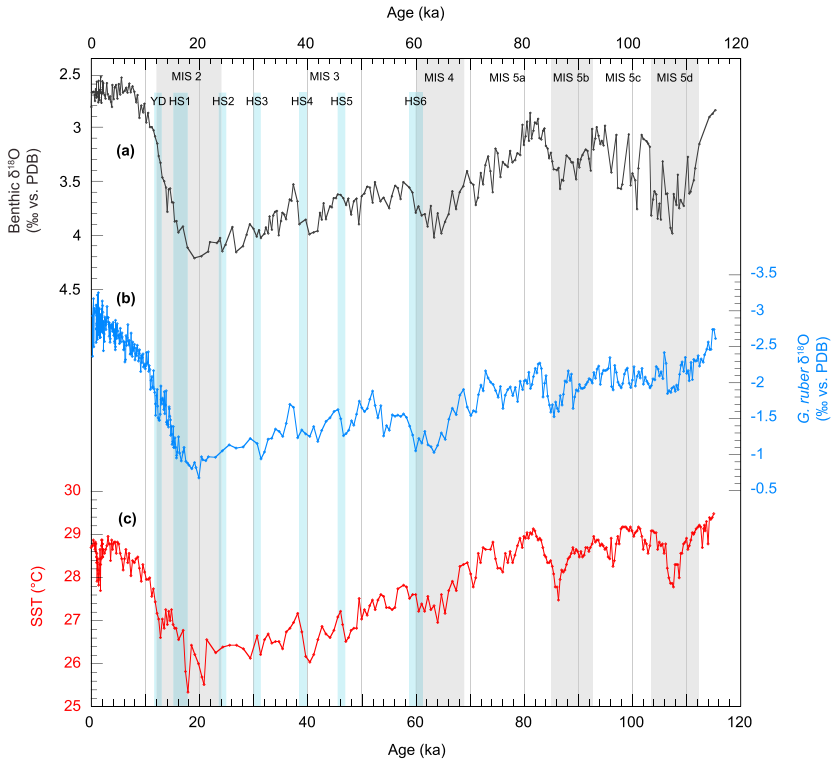

Figure 4. (a) Benthic $\delta^{18}O$ record of Core MD06-3075. (b) Planktonic $\delta^{18}O$ record of Core MD06-3075 based upon the surface dwelling foraminifera *G. ruber*. (c) $U^{K'}_{37}$-derived SST record of Core MD06-3075. Grey vertical bars indicate major marine isotope stages, blue vertical bars indicate HS1–HS6 and the YD.

in log(Fe/Ca) is noted consistent with the timing of HS1, followed by a decrease during the BA period, and a return to higher values in the YD. Log ratios plateau from 11 to 7 ka, prior to a substantial increase between 7 and 5 ka and an additional plateau in the late Holocene.

4.6. Primary Productivity

Primary productivity, inferred from counts of the coccolithophore *F. profunda*, shows variability between 130–220 gC/m^2/yr (*F. profunda* relative abundances of 22–53%), when using the calibration of *Beaufort et al.* [1997] (Figure 5). Lowest productivities are observed during MIS 5, with peaks and troughs demonstrating an antiphase relationship with log(Fe/Ca). MIS 4 is characterized by increased productivity, with a prominent peak occurring at 60 ka with a maximum value of 208 gC/m^2/yr. A general increasing trend is noted throughout MIS 3 and MIS 2, reaching maximum values during the BA period and subsequently decreasing steadily throughout the Younger Dryas and Holocene.

4.7. Carbonate Content

Carbonate content varies between 4.5 and 13% over the past 120 ka (Figure 5). Peaks and troughs in carbonate content generally follow a similar pattern to primary productivity. In MIS 5 two distinct peaks in carbonate content occur at ~80 and ~100 ka, contemporaneous with peaks in productivity. Values during MIS 3 fluctuate between 11 and 8%, and increase to the highest values during the LGM (12%) and BA period (13%). Carbonate content decreases steadily from the BA period to its minimum value of 4.5% in the late Holocene.

5. Discussion

5.1. Proxies of Paleoprecipitation in the WPWP

5.1.1. $\delta^{18}O_{sw}$ as a Proxy of Past Convective Activity

The deglacial evolution of *G. ruber* $\delta^{18}O$ from Core MD06-3075 is in agreement with previous Davao Gulf records [*Stott et al.*, 2002], indicating a decrease in $\delta^{18}O$ during Termination I on the order of ~2.2‰ (Figure 4 and Figure S2 in the supporting information). Only 1.0–1.2‰ of this variability can be attributed

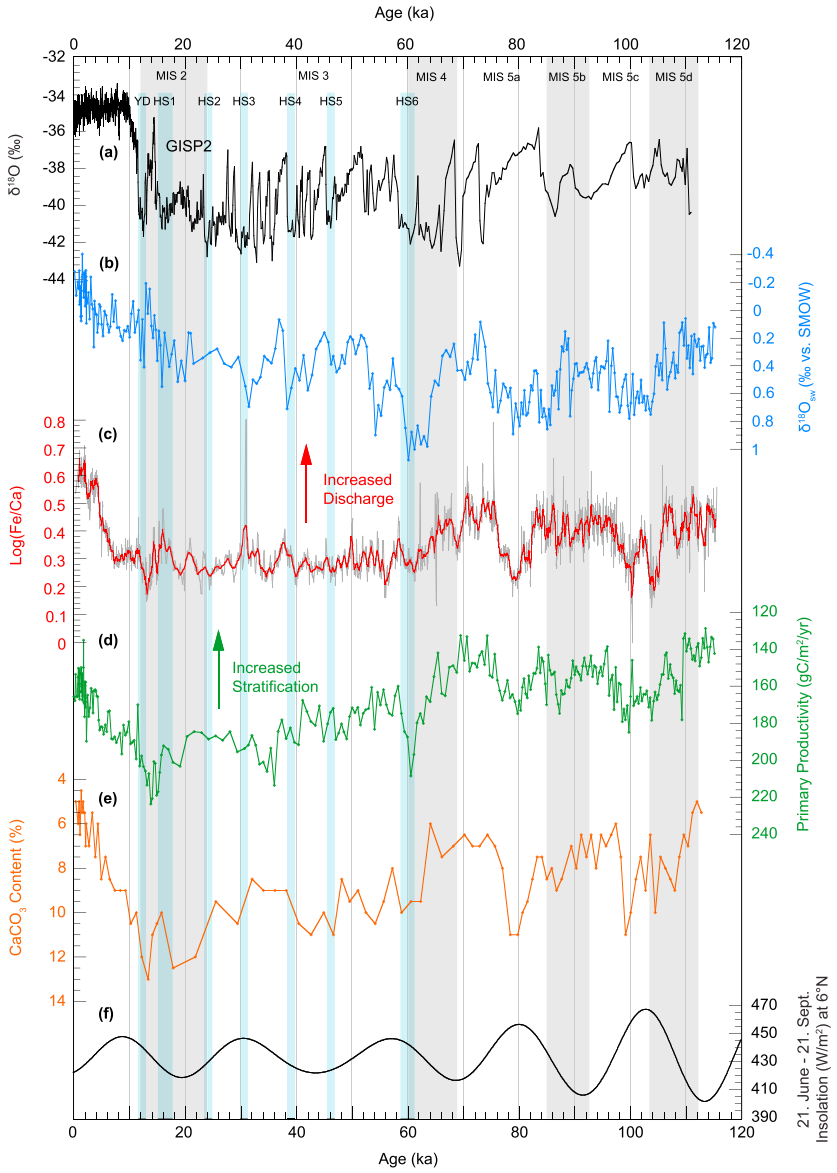

Figure 5. (a) Greenland (GISP2) ice core $\delta^{18}O$ [*Stuiver and Grootes*, 2000]. (b) Estimated ice volume-corrected $\delta^{18}O_{sw}$ from $\delta^{18}O$ measurements on *G. ruber* and $U^{K'}_{37}$-derived SSTs in Core MD06-3075. (c) XRF records of log(Fe/Ca) from Core MD06-3075. (d) Paleoproductivity records from Core MD06-3075 calculated from abundances of *F. profunda* using the equation of *Beaufort et al.* [1997]. Note inverted scale. (e) Calcium carbonate content (%) in Core MD06-3075. Note inverted scale. (f) Mean summer (21 June to 21 September) insolation at 6°N. Grey vertical bars indicate major marine isotope stages, blue vertical bars indicate HS1-HS6 and the YD.

to the global ice volume effect [*Fairbanks*, 1989; *Schrag et al.*, 2002], and the remaining 1.0–1.2‰ is thus accounted for by warming and hydrologic changes in the surface layer from the LGM to present. Observed linear correlations between $\delta^{18}O_{sw}$ and salinity [*Schmidt*, 1999] suggest that ice volume and temperature-corrected foraminiferal $\delta^{18}O_{sw}$ estimates have the potential to be employed as a proxy for paleosalinity of surface waters, linked to past changes in the balance of evaporation and precipitation. However, the relationship between $\delta^{18}O_{sw}$ and salinity is regionally dependent, exhibiting a global ~0.5‰ change in $\delta^{18}O_{sw}$ per unit change in practical salinity unit (psu) [*Schmidt*, 1999], which is reduced to ~0.3‰/psu in the tropics due to intense evaporation and transport processes [*LeGrande and Schmidt*, 2006]. Past changes in these relationships may also induce large uncertainties into paleosalinity estimations, making simple

$\delta^{18}O_{sw}$-salinity conversions unsuitable [LeGrande and Schmidt, 2011; *Leduc et al*., 2013]. Instead, $\delta^{18}O_{sw}$ may be better interpreted as a tracer of variability in the hydrologic cycle, influenced by large-scale changes in the transport of vapor, and balance of precipitation and evaporation in the Pacific Ocean [*Oppo et al*., 2007; *Gibbons et al*., 2014], in addition to small-scale processes linked to local precipitation effects.

Interpretation of $\delta^{18}O_{sw}$ in the WPWP is further complicated by the numerous marginal seas which influence local atmospheric and surface water circulation. For example, the $\delta^{18}O$ records of *G. ruber* from two cores situated in the Sulu Sea, ODP Site 769 [*Linsley*, 1996] and MD97-2141 [*Oppo et al*., 2003], exhibit a decrease of ~1.3‰ over Termination I, in line with the variability associated with the ice volume effect [*Fairbanks*, 1989; *Schrag et al*., 2002], but 0.9‰ lower than the variability measured in the Davao Gulf. These large differences in deglacial $\delta^{18}O$ amplitudes over relatively short distances in the WPWP cannot be reasonably explained by temperature differences and instead are likely influenced by variable exchange of fresh South China Sea surface waters over the deglacial period [*Oppo et al*., 2003]. This example highlights that the use of $\delta^{18}O$, and by extension $\delta^{18}O_{sw}$, as proxies for local hydrologic changes is highly subjective to regional sea level and surface water exchange mechanisms. This has widespread implications not only on marine records of $\delta^{18}O$ but also on the growing number of speleothem archives from the tropical Pacific and East Asian region [*Wang et al*., 2001, 2008; *Partin et al*., 2007; *Meckler et al*., 2012; *Carolin et al*., 2013; *Ayliffe et al*., 2013; *Denniston et al*., 2013], since source water $\delta^{18}O$ is an important control on $\delta^{18}O$ recorded in speleothems [*Breitenbach et al*., 2010; *Moerman et al*., 2013].

5.1.2. Proxies of Sedimentary Discharge

Associating XRF log ratios of terrigenous (i.e., Fe and Ti) versus marine (Ca) elements with continental sedimentary discharge relies on the assumption that dilution of Ca in the sediment matrix is driven primarily by variability in accumulation rates of the terrigenous fraction, and that additional processes for modulating Ca intensity (e.g., changes in the rate of biogenic carbonate production and deposition) are second order. Measurements of $CaCO_3$ content and paleoproductivity inferred from coccolithophore assemblages over the past 120 ka in Core MD06-3075 demonstrate an antiphase relationship with log(Fe/Ca) (Figure 5), suggesting that biogenic carbonate production may play a role in determining XRF log ratios at this locality. However, carbonate content is generally low, varying between 4.5 and 13%, and thus the terrigenous component represents the overwhelming majority of the sediment fraction in our core. In addition, the depth of the modern lysocline in the West Pacific sits at 3400 m [*Berger et al*., 1982], well below the depth of our core at 1878 m, and likely experienced only modest changes since the LGM [*Anderson and Archer*, 2002], suggesting that changes in carbonate dissolution and preservation had an insignificant effect on Ca variability. Individual test weights of *G. ruber*, which can be used as an indicator of dissolution, also show no significant trends over the deglacial portion of our record.

We therefore suggest that the proportions of Fe and Ca in our core were driven mainly by variability in the accumulation rates of terrigenous sediment driven by fluvial discharge of continental-sourced sediment into the Davao Gulf, with carbonate production acting as a second-order control. Variability in productivity in Core MD06-3075 was likely affected by transport of freshwater and detrital material into the surface waters of the Davao Gulf. During periods of high discharge, increased freshwater stratification and sediment loading of the upper surface waters could act to constrain productivity and deepen the nutricline, resulting in higher abundances of *F. profunda*. Additionally, increased silica input during periods of high discharge may result in blooms of predominantly siliceous phytoplankton [*Weldeab et al*., 2007], reducing productivity of calcareous species. This interpretation of log(Fe/Ca) records as an indicator of fluvial discharge is further supported by published pollen records from the same core [*Bian et al*., 2011] which suggest dry conditions during the LGM compared to the Holocene, as observed in our log(Fe/Ca) records, as well as reduced accumulation rates during the glacial portion of our record, which would be consistent with reduced sedimentary discharge. Taken together, our XRF log ratios and paleoproductivity reconstructions from the Davao Gulf present a robust picture of local rainfall variability over Mindanao during the past 120 ka.

5.2. WPWP Precipitation Over the Past 120 ka

5.2.1. Orbitally Paced Precipitation Changes at Mindanao

Orbital-scale trends of sedimentary discharge based upon log(Fe/Ca) ratios and paleoproductivity estimates suggest an antiphase relationship with local boreal summer insolation forcing—discharge is higher and productivity is lower during boreal summer insolation minima, and vice versa (Figure 6). This is corroborated by cross-spectral analysis, which shows a strong coherency (>95% confidence interval) of log(Fe/Ca) and

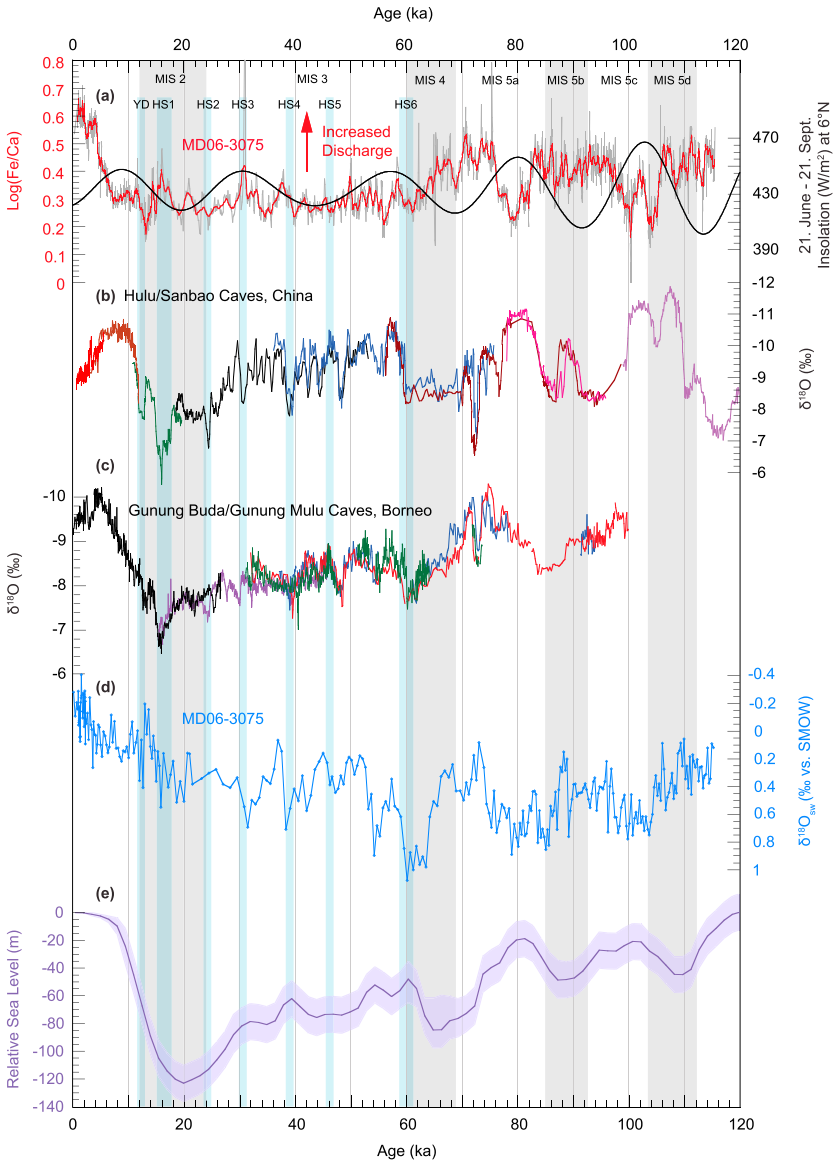

Figure 6. (a) XRF records of log(Fe/Ca) from Core MD06-3075 superimposed with mean boreal summer (21 June to 21 September) insolation at 6°N. (b) Composite speleothem $\delta^{18}O$ records from Hulu and Sanbao caves in China [*Wang et al.*, 2001, 2008]. (c) Composite speleothem $\delta^{18}O$ records from Gunung Mulu and Gunung Buda Caves in Borneo [*Partin et al.*, 2007; *Carolin et al.*, 2013]. (d) Estimated ice-volume corrected $\delta^{18}O_{sw}$ from $\delta^{18}O$ measurements on *G. ruber* and $U^{K'}_{37}$-derived SSTs in Core MD06-3075. (e) Relative sea level change based upon *Waelbroeck et al.* [2002]. Grey vertical bars indicate major marine isotope stages, blue vertical bars indicate HS1–HS6 and the YD.

boreal summer insolation (21 June–21 September) at 6°N in the precession band, with a phase spectrum indicating a lead of insolation over log(Fe/Ca) by ~176° (i.e., close to perfect antiphase) (supporting information Figure 4). The last interglacial period in particular is characterized by precessional-scale variability, which may be a result of the stronger precessional insolation forcing during this time interval. Trends of $\delta^{18}O_{sw}$ show general agreement with log(Fe/Ca) and paleoproductivity during the last interglacial period (Figure 5), with higher values during low sedimentary discharge periods between 65 to 60 ka, 82 to 75 ka, and 105 to 96 ka. However, the timing of some major shifts in $\delta^{18}O_{sw}$, for example, the prominent positive excursion centered at 85 ka, does not show entire agreement with log(Fe/Ca) and productivity records, and thus these proxies may be partly influenced by different factors.

Between the middle and end of MIS 4, a marked increase in productivity is observed, likely in response to reduced freshwater input (and thus reduced sedimentary discharge) combined with lower SSTs, which may have been a result of enhanced vertical mixing of the water column. In contrast to MIS 4 and 5, MIS 3 is defined by a rather muted response to orbital forcing, with low values of log(Fe/Ca) accompanied by increasing productivity indicating a long-term regional drying (Figure 5). This muted hydroclimate response at times of weakened precessional forcing in the WPWP has also been documented in speleothem records covering several late Pleistocence glacial-interglacial cycles in Borneo [*Meckler et al*., 2012], while log(Ti/Ca) records from the north of Papua New Guinea also show less pronounced precessional-scale variability during the last glacial period [*Tachikawa et al*., 2011]. However, it is interesting to note that despite the "dry" conditions inferred from log(Fe/Ca) and productivity records in Core MD06-3075, $\delta^{18}O_{sw}$ shows a long-term decreasing trend from the end of MIS 4 to the LGM. These differing trends likely reflect decoupling of local precipitation, which is more faithfully recorded in terrestrial proxies, versus changes in regional hydrology which are recorded in $\delta^{18}O_{sw}$.

Comparison of hydroclimate records from Core MD06-3075 with speleothem $\delta^{18}O$ records from Borneo [*Partin et al*., 2007; *Carolin et al*., 2013] and China [*Wang et al*., 2001, 2008] indicates that convection patterns are linked across the WPWP (Figure 6). A general antiphase relationship is observed between log(Fe/Ca) at Mindanao and speleothem $\delta^{18}O$ in China during MIS 5. During Northern Hemisphere summer insolation maxima, reduced $\delta^{18}O$ values in Chinese speleothems (interpreted as a strengthened EAM state) [*Wang et al*., 2001, 2008] are correlated with low log(Fe/Ca) values at Mindanao (interpreted as reduced runoff). In the modern day, both regions receive greater rainfall during the boreal summer when the ITCZ is located to the North, and thus this dipole-like pattern is not explained by modern analogies to a northward shift of the ITCZ. Instead, the precipitation pattern during MIS 5 suggests that increased northerly penetration of monsoon rainfall in response to Northern Hemisphere summer insolation maxima is balanced by reduced precipitation at Mindanao. However, such an antiphase pattern is not evident during the last glacial period and the Holocene, implying a different response during periods of weakened precessional forcing.

In contrast, speleothem $\delta^{18}O$ records from Borneo are shown to be in phase with boreal fall insolation [*Carolin et al*., 2013], despite their latitudinal position being only ~2° south of Core MD06-3075, implying different controls on hydrology in the marine versus land realm of the Indo-Pacific region. This finding is consistent with modeling studies that show regional sensitivity to the seasonal distribution of insolation in the tropical West Pacific [*Tierney et al*., 2012]. In addition, the pattern of ITCZ displacement as a response to past climate change may not have been globally or even regionally consistent, and larger meridional displacements could have occurred over small zonal extents [*McGee et al*., 2014]. Phase shifts between records of convection from Mindanao and those in Borneo, and a lack of response to precessional insolation forcing during the last glacial period is therefore further evidence that a simplistic view of homogenous ITCZ latitudinal migration driven by precession cannot fully explain changes in convective activity in the WPWP over the entire length of our record.

In the modern day, ENSO variability also has a significant impact on precipitation at Mindanao (Figure 2), thus we may expect that long-term changes in the mean ENSO state could have impacted past precipitation. A simplified modeling approach by *Clement et al*. [1999] highlighted the influence of the precessional cycle on ENSO variability; however, the proposed ENSO response in this model combined with the modern influence of ENSO at our core site (Figure 2) would suggest precipitation anomalies opposite in sign to our observed log (Fe/Ca) records. Attempts to reconstruct ENSO conditions in the late Pleistocene, for example, through reconstructions of cross-equatorial temperature gradients [e.g., *Lea et al*., 2000; *Koutavas et al*., 2002], have also lacked agreement on the magnitude or mechanisms of past ENSO variability, while little support for an ENSO signature has been found based upon $\delta^{18}O_{sw}$ reconstructions in the east and west Pacific occurring over the last deglacial period [*Leduc et al*., 2007; *Gibbons et al*., 2014].

The role of sea level changes has been recently highlighted as an important driver of the strength and position of the Walker circulation, where increased Sunda Shelf exposure during glacial sea level lowstands can act to reduce convective motion over the maritime continent [*DiNezio et al*., 2011; *DiNezio and Tierney*, 2013]. These findings may help to explain the muted response of precipitation to precessional forcing during the last glacial period, as sea level was lower and Sunda Shelf exposure was higher (Figure 6), which could have promoted widespread subsidence over the Indonesian landmass. This mechanism would be furthermore consistent with log(Ti/Ca) records from North of Papua New Guinea, which showed reduced

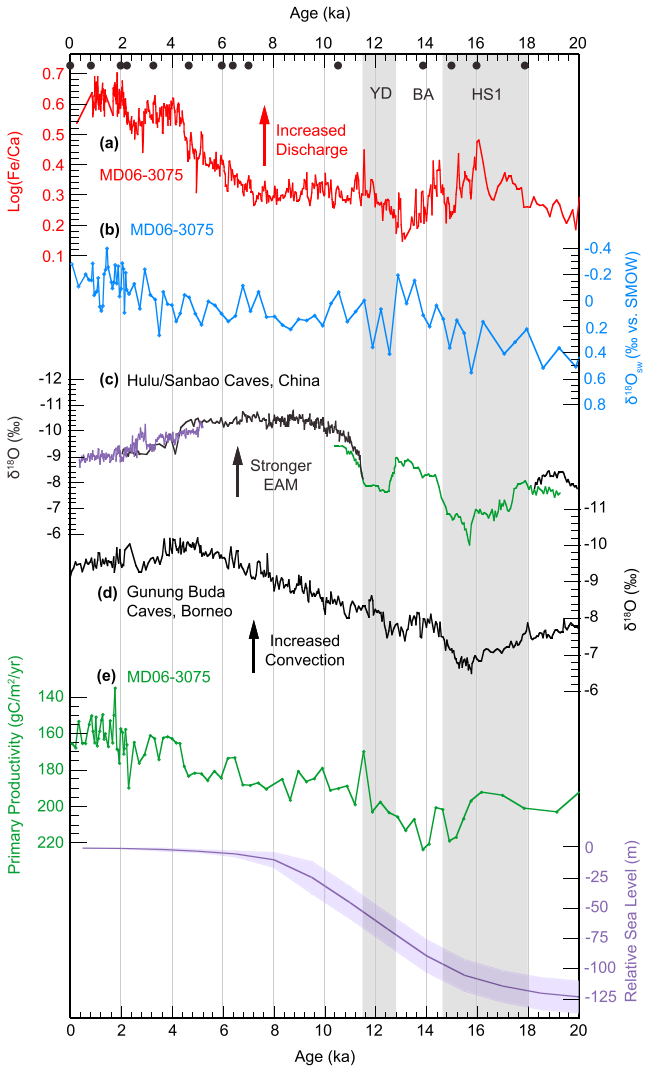

Figure 7. Expanded records covering the past 20 ka. Black dots indicate ^{14}C AMS dates used for age control. (a) XRF records of log(Fe/Ca) from Core MD06-3075. (b) Estimated $\delta^{18}O_{sw}$ from $\delta^{18}O$ measurements on *G. ruber* and $U^{K'}_{37}$-derived SSTs in Core MD06-3075. (c) Composite speleothem $\delta^{18}O$ records from Hulu and Sanbao caves in China [*Wang et al.*, 2001, 2008]. (d) Spliced speleothem $\delta^{18}O$ record from Gunung Buda Caves in Borneo [*Partin et al.*, 2007]. (e) Paleoproductivity records from Core MD06-3075 calculated from abundances of *F. profunda* using the equation of *Beaufort et al.* [1997]. Note inverted axis. (f) Relative sea level change based upon *Waelbroeck et al.* [2002].

values during the last glacial period when the shelf between Australia and Papua New Guinea was exposed [*Tachikawa et al.*, 2011]. However, with only few records of WPWP hydroclimate extending over multiple glacial-interglacial cycles, it remains a question as to whether the spatial pattern of convection is more consistent with changes associated with the Walker circulation versus changes occurring as a result of meridional ITCZ dynamics.

5.2.2. Suborbital Forcing of WPWP Hydroclimate

Records of log(Fe/Ca) and productivity in Core MD06-3075 do not show consistent responses to Heinrich stadials over MIS 3 (Figure 5). This may in part be due to reduced sedimentation rates and lower resolution in the glacial portion of our records, which does not allow identification of individual Heinrich stadials. The upper portion of our record (from the LGM to present day) has a tighter-constrained chronology via AMS ^{14}C dating, combined with a much higher temporal resolution (Figure 3), and thus we can therefore make inferences of millennial-scale variability over this period. HS1 is marked with an increase in log(Fe/Ca) and

reduced productivity, consistent with a period of increased sedimentary discharge, and therefore increased precipitation, at Mindanao (Figure 7). This trend reverses during the BA period. The regional pattern of convection changes during HS1, with increased precipitation at Mindanao and dry conditions in Borneo and China [*Wang et al*., 2001; *Partin et al*., 2007] is consistent with new modeling results presented by *Mohtadi et al*. [2014], which show that the climatic response to HS1 in the West Pacific is more complex than a simple southward shift of the rain belts associated with a southerly positioned ITCZ; while western and central Indonesia experienced drier conditions, the southern Philippines may have become wetter.

In contrast to log(Fe/Ca) and productivity records, $\delta^{18}O_{sw}$ shows generally higher values during HS1 and the YD than during the BA period, though we note divergence with the closely located $\delta^{18}O_{sw}$ record of *Stott et al*. [2002, 2007] which may be caused by different methods of SST reconstructions used to calculate $\delta^{18}O_{sw}$ (Figure S2 in the supporting information). Higher $\delta^{18}O_{sw}$ during HS1 and the YD than the BA period is a consistent signal observed across the WPWP in marine sediments [*Gibbons et al*., 2014], as well as in speleothem $\delta^{18}O$ records from both China [*Wang et al*., 2001] and Borneo [*Partin et al*., 2007] (Figure 7), which is further evidence that changes in $\delta^{18}O_{sw}$ are controlled primarily by large-scale reorganizations of the hydrologic cycle, linked on millennial timescales to Northern Hemisphere climate events.

6. Conclusions

Records of sedimentary discharge and productivity in Core MD06-3075 from the Davao Gulf, at the boundary between the Indonesian archipelago and the open West Pacific, are linked to local precipitation variability over the past 120 ka. During MIS 5, precipitation at Mindanao responds to precessional insolation forcing with highest precipitation noted during Northern Hemisphere insolation minima and vice versa. We suggest that two mechanisms were responsible for controlling orbital-scale variability in West Pacific precipitation: (1) latitudinal migrations of the mean ITCZ position driven by precessional cyclicity. During Northern Hemisphere insolation maxima, the summer position of the ITCZ migrates northward, inducing greater precipitation in China, which is balanced by reduced precipitation in the central WPWP region and (2) strengthening/weakening of the Walker circulation caused by changes in the hydrologic cycle and sea level. It is likely that these two mechanisms are tightly coupled, and resolving the relative importance of each component would require a greater number of precipitation records covering several late Quaternary precessional cycles in the WPWP. In the last glacial period, precipitation was suppressed and showed little orbital-scale variability, which we attribute to the reduced amplitude of precessional cyclicity, combined with increased subsidence of air masses over the exposed Sunda Shelf. Differing long-term trends observed in $\delta^{18}O_{sw}$ reconstructions in Core MD06-3075 likely reflect a composite of regional climatic processes, including changes in salinity, moisture sources, and transport pathways, not limited to local precipitation variability.

Acknowledgments

We thank the chief scientist, Carlo Laj, the captain and crew of R/V *Marion Dufresne*, Catherine Kissel, Yvon Balut, and the French Polar Institute for their effort and support during the Marco Polo 2 Cruise (IMAGES). We are grateful to Marie-Josée Nadeau and the Leibniz Laboratory team for AMS ^{14}C measurements, to Silvia Koch for technical assistance with $U^{K'}_{37}$ analysis, and to Ursula Röhl and the Marum Center for Marine Environmental Sciences (Bremen University) for XRF scanning. We also thank the Editor, Christopher Charles, and one anonymous reviewer for valuable and constructive comments that improved the quality of this manuscript. This research was carried out as part of the Throughflow Project, funded by the Marie Curie Actions Plan, Seventh Framework Programme (grant 237922). Additional funding was provided by DFG grant KU 649/26-1. Data presented in this paper are archived at www.pangaea.de.

References

Aitchison, J. (1982), The statistical analysis of compositional data, *J. R. Stat. Soc. Ser. B (Methodological)*, *44*(2), 139–177.

Anderson, D. M., and D. Archer (2002), Glacial-interglacial stability of ocean pH inferred from foraminifer dissolution rates, *Nature*, *416*(6876), 70–73, doi:10.1038/416070a.

Andruleit, H., and U. Rogalla (2002), Coccolithophores in surface sediments of the Arabian Sea in relation to environmental gradients in surface waters, *Mar. Geol.*, *186*(3), 505–526, doi:10.1016/S0025-3227(02)00312-2.

Antonov, J. I., D. Seidov, T. P. Boyer, R. A. Locarnini, A. V. Mishonov, H. E. Garcia, O. K. Baranova, M. M. Zweng, and D. R. Johnson (2010), *World Ocean Atlas 2009, Volume 2: Salinity*, NOAA Atlas NESDIS, vol. 69, edited by S. Levitus, pp. 1–184, U.S. Government Printing Office, Washington, D. C.

Arz, H. W., J. Pätzold, and G. Wefer (1998), Correlated millennial-scale changes in surface hydrography and terrigenous sediment yield inferred from last-glacial marine deposits off northeastern Brazil, *Quat. Res.*, *50*(2), 157–166, doi:10.1006/qres.1998.1992.

Ayliffe, L. K., et al. (2013), Rapid interhemispheric climate links via the Australian monsoon during the last deglaciation, *Nat. Commun.*, *4*, doi:10.1038/ncomms3908.

Beaufort, L., Y. Lancelot, P. Camberlin, O. Cayre, E. Vincent, F. Bassinot, and L. Labeyrie (1997), Insolation cycles as a major control of equatorial Indian Ocean primary production, *Science*, *278*(5342), 1451–1454, doi:10.1126/science.278.5342.1451.

Beaufort, L., T. de Garidel-Thoron, A. C. Mix, and N. G. Pisias (2001), ENSO-like forcing on oceanic primary production during the late Pleistocene, *Science*, *293*(5539), 2440–2444, doi:10.1126/science.293.5539.2440.

Bemis, B. E., H. J. Spero, J. Bijma, and D. W. Lea (1998), Reevaluation of the oxygen isotopic composition of planktonic foraminifera: Experimental results and revised paleotemperature equations, *Paleoceanography*, *13*(2), 150–160, doi:10.1029/98PA00070.

Berger, W. H., M. C. Bonneau, and F. L. Parker (1982), Foraminifera on the deep-sea floor-lysocline and dissolution rate, *Oceanol. Acta*, *5*(2), 249–258.

Bian, Y., Z. Jian, C. Weng, W. Kuhnt, T. Bolliet, and A. Holbourn (2011), A palynological and palaeoclimatological record from the southern Philippines since the Last Glacial Maximum, *Chin. Sci. Bull.*, *56*(22), 2359–2365, doi:10.1007/s11434-011-4573-1.

Bjerknes, J. (1969), Atmospheric teleconnections from the equatorial Pacific 1, *Mon. Weather Rev.*, *97*(3), 163–172.

Bolliet, T., A. Holbourn, W. Kuhnt, C. Laj, C. Kissel, L. Beaufort, M. Kienast, N. Andersen, and D. Garbe-Schönberg (2011), Mindanao Dome variability over the last 160 kyr: Episodic glacial cooling of the West Pacific Warm Pool, *Paleoceanography*, *26*, PA1208, doi:10.1029/2010PA001966.

Breitenbach, S. F., J. F. Adkins, H. Meyer, N. Marwan, K. K. Kumar, and G. H. Haug (2010), Strong influence of water vapor source dynamics on stable isotopes in precipitation observed in Southern Meghalaya, NE India, *Earth Planet. Sci. Lett.*, *292*(1), 212–220, doi:10.1016/j.epsl.2010.01.038.

Cane, M. A. (1998), A role for the tropical Pacific, *Science*, *282*(5386), 59–61, doi:10.1126/science.282.5386.59.

Carolin, S. A., K. M. Cobb, J. F. Adkins, B. Clark, J. L. Conroy, S. Lejau, J. Malang, and A. A. Tuen (2013), Varied response of western pacific hydrology to climate forcings over the last glacial period, *Science*, *340*(6140), 1564–1566, doi:10.1126/science.1233797.

Cheng, H., A. Sinha, X. Wang, F. W. Cruz, and R. L. Edwards (2012), The global paleomonsoon as seen through speleothem records from Asia and the Americas, *Clim. Dyn.*, *39*(5), 1045–1062, doi:10.1007/s00382-012-1363-7.

Clement, A. C., R. Seager, and M. A. Cane (1999), Orbital controls on the El Niño/Southern Oscillation and the tropical climate, *Paleoceanography*, *14*(4), 441–456, doi:10.1029/1999PA900013.

Cruz, F. W., S. J. Burns, I. Karmann, W. D. Sharp, M. Vuille, A. O. Cardoso, J. A. Ferrari, P. L. Silva Dias, and O. Viana (2005), Insolation-driven changes in atmospheric circulation over the past 116,000 years in subtropical Brazil, *Nature*, *434*(7029), 63–66, doi:10.1038/nature03365.

Dannenmann, S., B. K. Linsley, D. W. Oppo, Y. Rosenthal, and L. Beaufort (2003), East Asian monsoon forcing of suborbital variability in the Sulu Sea during marine isotope stage 3: Link to Northern Hemisphere climate, *Geochem., Geophys., Geosyst.*, *4*(1), 1–13, doi:10.1029/2002GC000390.

de Garidel-Thoron, T., Y. Rosenthal, L. Beaufort, E. Bard, C. Sonzogni, and A. C. Mix (2007), A multiproxy assessment of the western equatorial Pacific hydrography during the last 30 kyr, *Paleoceanography*, *22*, PA3204, doi:10.1029/2006PA001269.

Denniston, R. F., K. H. Wyrwoll, Y. Asmerom, V. J. Polyak, W. F. Humphrey, H. Cugley, D. Woods, Z. LaPointe, J. Peota, and E. Greaves (2013), North Atlantic forcing of millennial-scale Indo-Australian monsoon dynamics during the Last Glacial period, *Quat. Sci. Rev.*, *72*, 159–168, doi:10.1016/j.quascirev.2013.04.012.

DiNezio, P. N., and J. E. Tierney (2013), The effect of sea level on glacial Indo-Pacific climate, *Nat. Geosci.*, *6*, 485–491, doi:10.1038/ngeo1823.

DiNezio, P. N., A. Clement, G. A. Vecchi, B. Soden, A. J. Broccoli, B. L. Otto-Bliesner, and P. Braconnot (2011), The response of the Walker circulation to Last Glacial Maximum forcing: Implications for detection in proxies, *Paleoceanography*, *26*, PA3217, doi:10.1029/2010PA002083.

Donohoe, A., J. Marshall, D. Ferreira, and D. McGee (2013), The relationship between ITCZ location and cross-equatorial atmospheric heat transport: From the seasonal cycle to the last glacial maximum, *J. Clim.*, *26*(11), 3597–3618, doi:10.1175/JCLI-D-12-00467.1.

Fairbanks, R. G. (1989), A 17,000-year glacio-eustatic sea level record: Influence of glacial melting rates on the Younger Dryas event and deep-ocean circulation, *Nature*, *342*(6250), 637–642, doi:10.1038/342637a0.

Fairbanks, R. G., R. A. Mortlock, T. Chiu, L. Cao, A. Kaplan, T. P. Guilderson, T. W. Fairbanks, A. L. Bloom, P. M. Grootes, and M.-J. Nadeau (2005), Radiocarbon calibration curve spanning 0 to 50,000 years BP based on paired $^{230}Th/^{234}U/^{238}U$ and ^{14}C dates on pristine corals, *Quat. Sci. Rev.*, *24*(16), 1781–1796, doi:10.1016/j.quascirev.2005.04.007.

Gibbons, F. T., D. W. Oppo, M. Mohtadi, Y. Rosenthal, J. Cheng, Z. Liu, and B. K. Linsley (2014), Deglacial $\delta^{18}O$ and hydrologic variability in the tropical Pacific and Indian Oceans, *Earth Planet. Sci. Lett.*, *387*, 240–251, doi:10.1016/j.epsl.2013.11.032.

Griffiths, M., R. Drysdale, M. Gagan, J. Zhao, L. Ayliffe, J. Hellstrom, W. Hantoro, S. Frisia, Y. Feng, and I. Cartwright (2009), Increasing Australian-Indonesian monsoon rainfall linked to early Holocene sea-level rise, *Nat. Geosci.*, *2*(9), 636–639, doi:10.1038/ngeo605.

Hoerling, M. P., J. W. Hurrell, and T. Xu (2001), Tropical origins for recent North Atlantic climate change, *Science*, *292*(5514), 90–92, doi:10.1126/science.1058582.

International Atomic Energy Agency/World Meteorological Organization (2013), Global Network of Isotopes in Precipitation, The GNIP Database. [Available at http://www.iaea.org/water.]

Kashino, Y., M. Aoyama, T. Kawano, N. Hendiarti, Y. Anantasena, K. Muneyama, and H. Watanabe (1996), The water masses between Mindanao and New Guinea, *J. Geophys. Res. (1978–2012)*, *101*(C5), 12,391–12,400, doi:10.1029/95JC03797.

Koutavas, A., J. Lynch-Stieglitz, T. M. Marchitto, and J. P. Sachs (2002), El Niño-like pattern in ice age tropical Pacific sea surface temperature, *Science*, *297*(5579), 226–230, doi:10.1126/science.1072376.

Laj, C., and Shipboard Scientific Party (2006), Les rapports de campagnes a la mer: MD155-Marco Polo 2, IMAGES XIV cruise report, 11 juin au 6 juillet 2006, Publications de l'institut Polaire Francais, OCE/2006/06.

Lea, D. W., D. K. Pak, and H. J. Spero (2000), Climate impact of late Quaternary equatorial Pacific sea surface temperature variations, *Science*, *289*(5485), 1719–1724, doi:10.1126/science.289.5485.1719.

Leduc, G., L. Vidal, K. Tachikawa, F. Rostek, C. Sonzogni, L. Beaufort, and E. Bard (2007), Moisture transport across Central America as a positive feedback on abrupt climatic changes, *Nature*, *445*(7130), 908–911, doi:10.1038/nature05578.

Leduc, G., J. P. Sachs, O. E. Kawka, and R. R. Schneider (2013), Holocene changes in eastern equatorial Atlantic salinity as estimated by water isotopologues, *Earth Planet. Sci. Lett.*, *362*, 151–162, doi:10.1016/j.epsl.2012.12.003.

LeGrande, A. N., and G. A. Schmidt (2006), Global gridded data set of the oxygen isotopic composition in seawater, *Geophys. Res. Lett.*, *33*, L12604, doi:10.1029/2006GL026011.

Linsley, B. K. (1996), Oxygen-isotope record of sea level and climate variations in the Sulu Sea over the past 150,000 years, *Nature*, *380*, 234–237, doi:10.1038/380234a0.

Locarnini, R. A., A. V. Mishonov, J. I. Antonov, T. P. Boyer, H. E. Garcia, O. K. Baranova, M. M. Zweng, and D. R. Johnson (2010), *World Ocean Atlas 2009, Volume 1: Temperature*, NOAA Atlas NESDIS, vol. 68, edited by S. Levitus, pp. 1–184, U.S. Government Printing Office, Washington, D. C.

Marchitto, T. M., W. B. Curry, J. Lynch-Stieglitz, S. P. Bryan, K. M. Cobb, and D. C. Lund (2014), Improved oxygen isotope temperature calibrations for cosmopolitan benthic foraminifera, *Geochim. Cosmochim. Acta*, *130*, 1–11, doi:10.1016/j.gca.2013.12.034.

Martinez, I., L. Keigwin, T. T. Barrows, Y. Yokoyama, and J. Southon (2003), La Niña like conditions in the eastern equatorial Pacific and a stronger Choco jet in the northern Andes during the last glaciation, *Paleoceanography*, *18*(2, 1033), doi:10.1029/2002PA000877.

McGee, D., A. Donohoe, J. Marshall, and D. Ferreira (2014), Changes in ITCZ location and cross-equatorial heat transport at the Last Glacial Maximum, Heinrich Stadial 1, and the mid-Holocene, *Earth Planet. Sci. Lett.*, *390*, 69–79, doi:10.1016/j.epsl.2013.12.043.

Meckler, A., M. Clarkson, K. Cobb, H. Sodemann, and J. Adkins (2012), Interglacial hydroclimate in the tropical West Pacific through the Late Pleistocene, *Science*, *336*(6086), 1301–1304, doi:10.1126/science.1218340.

Medina-Elizalde, M. N., and D. W. Lea (2005), The mid-Pleistocene transition in the Tropical Pacific, *Science*, *310*(5750), 1009–1012, doi:10.1126/science.1115933.

Merlis, T. M., T. Schneider, S. Bordoni, and I. Eisenman (2013), Hadley circulation response to orbital precession. Part I: Aquaplanets, *J. Clim.*, *26*(3), 740–753, doi:10.1175/JCLI-D-11-00716.1.

Moerman, J. W., K. M. Cobb, J. F. Adkins, H. Sodemann, B. Clark, and A. A. Tuen (2013), Diurnal to interannual rainfall $\delta^{18}O$ variations in northern Borneo driven by regional hydrology, *Earth Planet. Sci. Lett.*, *369*, 108–119, doi:10.1016/j.epsl.2013.03.014.

Mohtadi, M., M. Prange, D. W. Oppo, R. De Pol-Holz, U. Merkel, X. Zhang, S. Steinke, and A. Lückge (2014), North Atlantic forcing of tropical Indian Ocean climate, *Nature*, *509*(7498), 76–80, doi:10.1038/nature13196.

Molfino, B., and A. McIntyre (1990), Nutricline variation in the equatorial Atlantic coincident with the Younger Dryas, *Paleoceanography*, *5*(6), 997–1008, doi:10.1029/PA005i006p00997.

Müller, G., and M. Gastner (1971), The 'Karbonat-Bombe', a simple device for the determination of carbonate content in sediment, soils, and other materials, *Neues Jahrbuch für Mineralogie - Monatshefte*, *10*, 466–469.

Nadeau, M.-J., M. Schleicher, P. Grootes, H. Erlenkeuser, A. Gottdang, D. Mous, M. Sarnthein, and H. Willkomm (1997), The Leibniz-Labor AMS facility at the Christian-Albrechts University, Kiel, Germany, *Nucl. Instrum. Methods Phys. Res., Sect. B*, *123*(1), 22–30, doi:10.1016/S0168-583X(96)00730-6.

Oppo, D. W., G. A. Schmidt, and A. N. LeGrande (2007), Seawater isotope constraints on tropical hydrology during the Holocene, *Geophys. Res. Lett.*, *34*, L13701, doi:10.1029/2007GL030017.

Oppo, D., B. Linsley, Y. Rosenthal, S. Dannenmann, and L. Beaufort (2003), Orbital and suborbital climate variability in the Sulu Sea, western tropical Pacific, *Geochem. Geophys. Geosyst.*, *4*(1), 1–20, doi:10.1029/2001GC000260.

Partin, J. W., K. M. Cobb, J. F. Adkins, B. Clark, and D. P. Fernandez (2007), Millennial-scale trends in west Pacific warm pool hydrology since the Last Glacial Maximum, *Nature*, *449*(7161), 452–455, doi:10.1038/nature06164.

Qu, T., H. Mitsudera, and T. Yamagata (1999), A climatology of the circulation and water mass distribution near the Philippine Coast*, *J. Phys. Oceanogr.*, *29*(7), 1488–1505.

Rincón-Martínez, D., F. Lamy, S. Contreras, G. Leduc, E. Bard, C. Saukel, T. Blanz, A. Mackensen, and R. Tiedemann (2010), More humid interglacials in Ecuador during the past 500 kyr linked to latitudinal shifts of the equatorial front and the Intertropical Convergence Zone in the eastern tropical Pacific, *Paleoceanography*, *25*, PA2210, doi:10.1029/2009PA001868.

Ropelewski, C. F., and M. S. Halpert (1987), Global and regional scale precipitation patterns associated with the El Niño/Southern oscillation, *Mon. Weather Rev.*, *115*, 1606–1626.

Ruth, U., J.-M. Barnola, J. Beer, M. Bigler, T. Blunier, E. Castellano, H. Fischer, F. Fundel, P. Huybrechts, and P. Kaufmann (2007), "EDML1": A chronology for the EPICA deep ice core from Dronning Maud Land, Antarctica, over the last 150 000 years, *Clim. Past Discuss.*, *3*(2), 549–574, doi:10.5194/cp-3-475-2007.

Saikku, R., L. Stott, and R. Thunell (2009), A bi-polar signal recorded in the western tropical Pacific: Northern and Southern Hemisphere climate records from the Pacific warm pool during the last Ice Age, *Quat. Sci. Rev.*, *28*(23), 2374–2385, doi:10.1016/j.quascirev.2009.05.007.

Schleicher, M., P. Grootes, M.-J. Nadeau, and A. Schoon (1998), The carbonate ^{14}C background and its components at the Leibniz AMS facility, *Radiocarbon*, *40*(1), 85–93.

Schmidt, G. A. (1999), Forward modeling of carbonate proxy data from planktonic foraminifera using oxygen isotope tracers in a global ocean model, *Paleoceanography*, *14*(4), 482–497, doi:10.1029/1999PA900025.

Schneider, T., T. Bischoff, and G. H. Haug (2014), Migrations and dynamics of the intertropical convergence zone, *Nature*, *513*(7516), 45–53, doi:10.1038/nature13636.

Schrag, D. P., J. F. Adkins, K. McIntyre, J. L. Alexander, D. A. Hodell, C. D. Charles, and J. F. McManus (2002), The oxygen isotopic composition of seawater during the Last Glacial Maximum, *Quat. Sci. Rev.*, *21*(1), 331–342, doi:10.1016/s0277-3791(01)00110-x.

Sonzogni, C., E. Bard, F. Rostek, D. Dollfus, A. Rosell-Melé, and G. Eglinton (1997), Temperature and salinity effects on alkenone ratios measured in surface sediments from the Indian Ocean, *Quat. Res.*, *47*(3), 344–355, doi:10.1006/qres.1997.1885.

Stott, L., C. Poulsen, S. Lund, and R. Thunell (2002), Super ENSO and global climate oscillations at millennial time scales, *Science*, *297*(5579), 222–226, doi:10.1126/science.1071627.

Stott, L., A. Timmermann, and R. Thunell (2007), Southern hemisphere and deep-sea warming led deglacial atmospheric CO_2 rise and tropical warming, *Science*, *318*(5849), 435–438, doi:10.1126/science.1143791.

Stuiver, M., and P. M. Grootes (2000), GISP2 oxygen isotope ratios, *Quat. Res.*, *53*(3), 277–284, doi:10.1006/qres.2000.2127.

Széréméta, N., F. Bassinot, Y. Balut, L. Labeyrie, and M. Pagel (2004), Oversampling of sedimentary series collected by giant piston corer: Evidence and corrections based on 3.5-kHz chirp profiles, *Paleoceanography*, *19*, PA1005, doi:10.1029/2002PA000795.

Tachikawa, K., O. Cartapanis, L. Vidal, L. Beaufort, T. Barlyaeva, and E. Bard (2011), The precession phase of hydrological variability in the Western Pacific Warm Pool during the past 400 ka, *Quat. Sci. Rev.*, *30*(25), 3716–3727, doi:10.1016/j.quascirev.2011.09.016.

Tierney, J. E., D. W. Oppo, A. N. LeGrande, Y. Huang, Y. Rosenthal, and B. K. Linsley (2012), The influence of Indian Ocean atmospheric circulation on Warm Pool hydroclimate during the Holocene epoch, *J. Geophys. Res.*, *117*, D19108, doi:10.1029/2012JD018060.

Timmermann, A., J. Sachs, and O. Elison Timm (2014), Assessing divergent SST behavior during the last 21 ka derived from alkenones and G.ruber-Mg/Ca in the equatorial Pacific, *Paleoceanography*, *29*, 680–696, doi:10.1002/2013PA002598.

Tjallingii, R., U. Röhl, M. Kölling, and T. Bickert (2007), Influence of the water content on X-ray fluorescence core-scanning measurements in soft marine sediments, *Geochem. Geophys. Geosyst.*, *8*, Q02004, doi:10.1029/2006GC001393.

Toole, J. M., R. C. Millard, Z. Wang, and S. Pu (1990), Observations of the Pacific North Equatorial Current Bifurcation at the Philippine Coast, *J. Phys. Oceanogr.*, *20*, 307–318.

Tudhope, A. W., C. P. Chilcott, M. T. McCulloch, E. R. Cook, J. Chapell, R. M. Ellam, D. W. Lea, J. M. Lough, and G. B. Shimmield (2001), Variability in the El Niño-Southern Oscillation through a glacial-interglacial cycle, *Science*, *291*(5508), 1511–1517, doi:10.1126/science.1057969.

Turney, C. S., A. P. Kershaw, S. C. Clemens, N. Branch, P. T. Moss, and L. K. Fifield (2004), Millennial and orbital variations of El Niño/Southern Oscillation and high-latitude climate in the last glacial period, *Nature*, *428*(6980), 306–310, doi:10.1038/nature02386.

Waelbroeck, C., L. Labeyrie, E. Michel, J. C. Duplessy, J. F. McManus, K. Lambeck, E. Balbon, and M. Labracherie (2002), Sea-level and deep water temperature changes derived from benthic foraminifera isotopic records, *Quat. Sci. Rev.*, *21*, 295–305, doi:10.1016/S0277-3791(01)00101-9.

Waliser, D. E., and C. Gautier (1993), A satellite-derived climatology of the ITCZ, *J. Clim.*, *6*(11), 2162–2174.

Wang, X., A. S. Auler, R. L. Edwards, H. Cheng, E. Ito, Y. Wang, X. Kong, and M. Solheid (2007), Millennial-scale precipitation changes in southern Brazil over the past 90,000 years, *Geophys. Res. Lett.*, *34*, L23701, doi:10.1029/2007GL031149.

Wang, Y., H. Cheng, R. L. Edwards, Z. An, J. Wu, C.-C. Shen, and J. A. Dorale (2001), A high-resolution absolute-dated late Pleistocene monsoon record from Hulu Cave, China, *Science*, *294*(5550), 2345–2348, doi:10.1126/science.1064618.

Wang, Y., H. Cheng, R. L. Edwards, X. Kong, X. Shao, S. Chen, J. Wu, X. Jiang, X. Wang, and Z. An (2008), Millennial-and orbital-scale changes in the East Asian monsoon over the past 224,000 years, *Nature*, *451*(7182), 1090–1093, doi:10.1038/nature06692.

Weldeab, S., D. W. Lea, R. R. Schneider, and N. Andersen (2007), 155,000 years of West African monsoon and ocean thermal evolution, *Science*, *316*(5829), 1303–1307, doi:10.1126/science.1140461.

Weltje, G. J., and R. Tjallingii (2008), Calibration of XRF core scanners for quantitative geochemical logging of sediment cores: Theory and application, *Earth Planet. Sci. Lett.*, *274*(3), 423–438, doi:10.1016/j.epsl.2008.07.054.

Xie, P., and P. A. Arkin (1997), Global precipitation: A 17-year monthly analysis based on gauge observations, satellite estimates, and numerical model outputs, *Bull. Am. Meteorol. Soc.*, *78*, 2539–2558.